Spectroscopy, Metastability, and Single and Double Ionization of AlCl

V. Brites,[†] D. Hammoutène,*[,‡] and M. Hochlaf*[,†]

Université Paris-Est, Laboratoire Modélisation et Simulation Multi Echelle, MSME FRE 3160 CNRS, 5 bd Descartes, 77454 Marne-la-Vallée, France, and Laboratoire de Thermodynamique et Modélisation Moléculaire, Faculté de Chimie, USTHB, BP32 El Alia, 16111 Bab Ezzouar, Alger, Algeria

Received: June 23, 2008; Revised Manuscript Received: October 14, 2008

Large calculations are done to investigate the valence and inner-valence electronic states of aluminum monochloride and its cationic species $AlCl^+$ and $AlCl^{2+}$, allowing their definite assignment. This concerns particularly the computations of the potential-energy curves of the electronic states of these species and their spin−orbit couplings and transition moments. An accurate set of spectroscopic constants for these species is also deduced. For the neutral molecule, our calculations show that the lifetimes of the AlCl $A^1\Pi$ $v' \geq 10$ levels are reduced to the 0.1−0.01 ps time scale because of spin−orbit induced predissociation processes and by tunneling through the potential barrier of the A state. Our potential curves for the ground state of AlCl and those of the cationic and dicationic species are also used for predicting the single and double ionization spectrum of AlCl. For both the cation and the dication, long-lived rovibrational levels are predicted.

1. Introduction

In 1987, Cernicharo and Guélin positively identified the neutral AlCl molecule in the carbon rich star IRC+10216 by microwave spectroscopy.[1] It was also positively identified by McGregor et al.[2] in the ultraviolet spectra of plumes from solid rockets. In the laboratory, AlCl was studied first by Bhaduri and Fowler[3] and by Mahanti[4] in 1934. Several experimental and theoretical investigations treating aluminum chloride followed these initial observations. Indeed, the structure and spectroscopic properties of the electronic ground state $X^1\Sigma^+$ of AlCl are well-known due to rotational transitions in the millimeter region[5−7] and later from a high-resolution emission spectrum of AlCl at 20 μm by Hedderich et al.[8] It is also established that the ground state does possess a deep potential, which is associated with the strong ionic character of the bonding in this molecule. A dissociation energy of $D_0 = 5.25 \pm 0.01$ eV[9,10] is estimated first from thermochemical measurements[9] and then from the optical experimental data of Ram et al.[10] Studies of the AlCl electronic excited states consist mainly of absorption and emission spectra from the first singlet−singlet (i.e., A−X), triplet−triplet (b−a), and triplet−singlet (a−X) systems.[4,8,9,11−14] The analysis of these spectra gives insight into the nature of these electronic states and has been used to deduce a set of accurate spectroscopic constants. Furthermore, a rapid predissociation of the AlCl $A^1\Pi$ $v' \geq 10$ levels was noticed. The highly excited states of AlCl lying at 24 000−60 000 cm^{-1} above the ground state were investigated using 1 + 2, 2 + 1, 2 + 2, 3 + 1, and 3 + 2 resonance-enhanced multiphoton ionization spectroscopy,[15] where Rydberg series converging to the $AlCl^+$ ground state were clearly identified. Theoretically, the configuration interaction treatments by Langhoff et al.[16] confirmed the assignments of the lowest singlet electronic states but proposed other attributions for some of the triplets. These authors concluded that the $0 \leq v' \leq 9$ $A^1\Pi$ levels are depleted mainly by fluorescence to the ground electronic state and that the $A^1\Pi$ state presents a potential barrier against dissociation into $Al(^2P_u) + Cl(^2P_u)$.

Concerning the $AlCl^+$ cation, reactions between Al^+ and Cl_2 have yielded optical emission spectra through the chemiluminescence of the $AlCl^+$ product.[17] Analysis of these spectra offers insight into the pattern of the lowest doublet electronic states. Theoretically, the four lowest doublet electronic states of $AlCl^+$, namely, $X^2\Sigma^+$, $A^2\Pi$, $B^2\Sigma^+$, and $C^2\Pi$, were calculated at the cc-pVQZ/CASSCF/MRCI level of theory,[18] confirming the assignment proposed in ref 17. It is worth citing also the earlier high-temperature (at 1000 K) theoretical photoelectron spectrum of AlCl by Berkowitz and Dehmer,[19] which is obtained using combined ab initio and semiempirical approaches. This spectrum consists of a first band, more or less structured, between 8 and 9 eV corresponding to the $AlCl^+(X^2\Sigma^+) + e^- \leftarrow AlCl(X^1\Sigma^+) + h\nu$ photoionization transition, followed by a large band spanning from 10 to 12 eV because of $AlCl^+(A^2\Pi) + e^- \leftarrow AlCl(X^1\Sigma^+) + h\nu$ photoionization transition.

As stated above, huge amounts of data are available for the neutral AlCl species, especially in its electronic ground state. Nevertheless, several features on its spectroscopy and dynamics remain unexplained. For instance, the assignment of the AlCl electronic states was the subject of several controversies in the literature and is not definitely established yet. Moreover, only the bound electronic states of AlCl are investigated in the extensive theoretical work of Langhoff et al.,[16] and nothing is said there concerning the repulsive states that can be involved, at least, during the predissociation processes. The situation is more critical for the cation, for which only the lowest doublets are studied. Nothing is available in the literature concerning the higher spin multiplicity electronic states, yet some of them correlate at long internuclear distances to the lowest dissociation limits as well as the doublet electronic states. These unknown electronic states could play crucial roles for the metastability of the doublets. Finally, no data are found in the literature treating the $AlCl^{2+}$ dication. This dication should be thermodynamically stable as demonstrated for its isovalent AlF^{2+} molecule, which has been successfully identified in the laboratory.[20]

* To whom correspondence should be addressed. E-mail: dhammoutene@yahoo.fr (D. H.), hochlaf@univ-mlv.fr (M. H.).
† Université Paris-Est.
‡ Laboratoire de Thermodynamique et Modélisation Moléculaire.

10.1021/jp805508f CCC: $40.75
Published on Web 11/21/2008

To fill the gap in our understanding of the structure, the spectroscopy, and the metastability of aluminum chloride in the gas phase, large ab initio calculations are performed presently dealing with the electronic states of AlCl, $AlCl^+$, and $AlCl^{2+}$. Highly correlated wave functions are used to deduce the transition moments and the spin−orbit coupling matrix elements between their respective electronic states. A set of accurate spectroscopic data is then deduced for the bound electronic states of AlCl, $AlCl^+$, and $AlCl^{2+}$. For some of the excited electronic states, rapid spin−orbit predissociation processes are identified. Finally, our potential curves of $AlCl^+$ and $AlCl^{2+}$ together with the $AlCl(X^1\Sigma^+)$ are used to predict the single and double ionization spectra of aluminum chloride.

2. Computational Methods

a. Electronic Calculations. Previous theoretical treatments of metallic-bearing compounds have pointed out the importance of electron correlation for a good description of their electronic states and properties. Only large atomic basis sets together with configuration interaction methods are expected to provide accurate data for metallic systems. In these calculations, the recently developed complete cc-pwCV5Z basis sets for aluminum and chlorine atoms were used.[21,22] This resulted in 362 contracted Gaussian functions to be treated. As shown by Peterson and Dunning, this basis set adequately describes both core−core and core−valence correlations. The electronic structure calculations were performed using the full valence complete active space self-consistent field (CASSCF) approach[23] followed by the internally contracted multireference configuration interaction (MRCI) technique.[24,25] Both of them are implemented in the *MOLPRO* program suite.[26] In CASSCF, all electronic states having the same spin multiplicity were averaged together with equal weights using the *MOLPRO* state averaging procedure. The calculations were carried out in the C_{2v} point group where the B_1 and B_2 representations were equivalently described. All valence molecular orbitals were considered in the CASSCF active space. Using these wave functions, the transition moment matrix elements were evaluated. At the MRCI level of theory, all configurations state functions (CSFs) from the CASSCF wave functions were taken as a reference. When computing the singlet electronic states of AlCl, this leads to more than 6×10^7 uncontracted CSFs to be considered in each symmetry of the C_{2v} point group. Then our PECs are incorporated into perturbative and variational treatment of the nuclear motion problem using the method of Cooley.[27] The spectroscopic constants in the following tables were obtained using the derivatives at the minimum energy distances and standard perturbation theory.

In the following, the energies including the Davidson correction (MRCI+Q)[28] are considered for better accuracy. Our potential-energy curves for AlCl, $AlCl^+$, and $AlCl^{2+}$ are given relative to the energy at the minimum of the electronic ground state AlCl ($X^1\Sigma^+$). The accuracy of the relative energy position of these curves is expected to be better than 0.1 eV for such large electronic calculations. Readers are referred to similar works on other metallic-bearing compounds for further details.[29,30] Finally, we would like to point out that the uncertainties quoted below correspond to 1σ deviation.

b. Spin−Orbit Calculations. The spin−orbit matrix elements needed for these calculations were evaluated in Cartesian coordinates over the CASSCF wave functions using a smaller basis set (i.e., the spdf cc-pVQZ basis subset[31]). At this level of theory, the spin−orbit constants of $Cl(^2P_u)$ and of $Cl^+(^3P_g)$ were computed to be 551.2 and 633.9 cm^{-1}, respectively. These ab initio values differ by less than 6% from those deduced experimentally,[32] which is the expected accuracy of such computations. For simplicity, only the spin−orbit integral evolutions that are needed presently in the discussion are given. The remaining couplings can be sent on request.

c. Lifetime Calculations. The radiative lifetimes are calculated using our PECs and our transition moment matrix elements and the *LEVEL* program of Le Roy.[33] The predissociation lifetimes of some electronic states of AlCl and $AlCl^{2+}$ were computed using the BCONT code of Le Roy,[34] which considers the isoenergetic predissociation from a discrete (v,J) rovibrational level of a bound potential-energy curve into the continuum of a repulsive electronic state whose asymptote is lying energetically below this (v,J). In these calculations, the potential-energy curves of both electronic states and their mutual spin−orbit coupling are incorporated and the predissociation rates are deduced by the Fermi Golden Rule formula.

3. Results and Discussion

a. AlCl. Table 1 gives the dominant electron configurations of the electronic states depicted in Figure 1 together with their vertical excitation energies with respect to the AlCl $X^1\Sigma^+$ minimum. These electronic states correspond mostly to the promotion of an electron from a valence or an inner-valence molecular orbital (MO) into the vacant 4π or 10σ molecular orbitals. These electronic states converge into the two lowest dissociation limits {i.e., $Al(^2P_u)$ + $Cl(^2P_u)$ and $Al^+(^1S_g)$ + $Cl^-(^1S_g)$}. The $Al(^2P_u)$ + $Cl(^2P_u)$ asymptote was located using our $AlCl(X^1\Sigma^+)$ D_0 dissociation energy computed at the MRCI + Q level of theory. This quantity is evaluated to be 5.25 ± 0.1 eV, in close agreement with the experimental determination of $D_0 = 5.25 \pm 0.01$ eV.[9,10] The ionic asymptote is located using the ionization energy of aluminum and the electron affinity of chlorine and an adequate thermochemical cycle.[35]

In addition to the known $X^1\Sigma^+$, $a^3\Pi$, and $A^1\Pi$ bound electronic states, a bound ionic state (i.e., the $3^1\Sigma^+$) is found. This singlet correlates solely to the second dissociation limit. It possesses an equilibrium distance for large AlCl distances (∼5.5 Å). A D_e dissociation energy of ∼2 eV is computed for this electronic state. The long-range potential well of the $3^1\Sigma^+$ state is found to be due to avoided crossings between the $^1\Sigma^+$ electronic states lying in the 0−8 eV energy range (cf. Figure 1 for more details). For $A^1\Pi$, our computations confirm the presence of a potential barrier against dissociation into $Al(^2P_u)$ + $Cl(^2P_u)$. This has been already noticed in the theoretical work of Langhoff et al.[16] (cf. Figure 2). In the 4.4−7.3 eV energy range, a high density of electronic states is remarkable (cf. Figure 1). Such a high density of states is expected to cause mixing of the electronic wave functions of these electronic states at their avoided crossings (cf. the ones between the $^1\Sigma^+$ states) and via Coriolis interactions (e.g., between the Σ and Π electronic states having the same spin multiplicities) and via spin−orbit couplings (below).

In this paragraph, we will be considering the assignment of the electronic states of AlCl in light of our new calculations. Indeed, some of them have been mis-assigned in the literature. For instance, the b−a triplet system was first thought to be due to a $^3\Sigma^+-^3\Pi$ emission by Sharma,[13] which was confirmed in 1988 by the ab initio computations of Langhoff et al.[16] but was invalidated one year later by Mahieu et al.[12] These authors attributed this emission to a $^3\Delta-^3\Pi$ system rather than to $^3\Sigma^+-^3\Pi$. Our large computations confirm once more the earlier attribution because of: 1) The vertical excitation energy of the $b^3\Sigma^+$ (∼5.50 eV, cf. Table 1) coincides with the theoretical energy computed by Langhoff et al. (5.43 eV) and that of 5.396

TABLE 1: Dominant Electronic Configurations of the AlCl, $AlCl^+$, and $AlCl^{2+}$ Electronic States Investigated Presently[a]

AlCl			$AlCl^+$			$AlCl^{2+}$		
state	electronic configuration	T	state	electronic configuration	T	state	electronic configuration	T
$X^1\Sigma^+$	$8\sigma^2 3\pi^4 9\sigma^2$	0.0	$X^2\Sigma^+$	$8\sigma^2 3\pi^4 9\sigma^1$	9.37	$X^1\Sigma^+$	$8\sigma^2 3\pi^4$	26.46
$a^3\Pi$	$8\sigma^2 3\pi^4 9\sigma^1 4\pi^1$	3.04	$A^2\Pi$	$8\sigma^2 3\pi^3 9\sigma^2$	11.92	$1^3\Pi$	$8\sigma^2 3\pi^3 9\sigma^1$	27.32
$A^1\Pi$	$8\sigma^2 3\pi^4 9\sigma^1 4\pi^1$	4.81	$B^2\Sigma^+$	$8\sigma^1 3\pi^4 9\sigma^2$	14.05	$1^1\Pi$	$8\sigma^2 3\pi^3 9\sigma^1$	27.50
$b^3\Sigma^+$	$8\sigma^2 3\pi^4 9\sigma^1 10\sigma^1$	5.50	$C^2\Pi$	$8\sigma^2 3\pi^4 9\sigma^0 4\pi^1$	14.17	$1^3\Sigma^+$	$8\sigma^1 3\pi^4 9\sigma^1$	29.42
$2^3\Sigma^+$	$8\sigma^2 3\pi^3 9\sigma^2 4\pi^1$	6.45	$1^4\Sigma^+$	$8\sigma^2 3\pi^3 9\sigma^1 4\pi^1$	14.91	$2^1\Sigma^+$	$8\sigma^1 3\pi^4 9\sigma^1$	31.03
$1^3\Delta$	$8\sigma^2 3\pi^3 9\sigma^2 4\pi^1$	6.64	$1^4\Delta$	$8\sigma^2 3\pi^3 9\sigma^1 4\pi^1$	15.12	$2^3\Sigma^+$	$8\sigma^2 3\pi^3 9\sigma^0 4\pi^1$	32.00
$2^1\Sigma^+$	$8\sigma^2 3\pi^4 9\sigma^1 10\sigma^1$ and $8\sigma^2 3\pi^3 9\sigma^2 4\pi^1$	6.71	$1^4\Sigma^-$	$8\sigma^2 3\pi^3 9\sigma^1 4\pi^1$	15.30	$1^3\Sigma^-$	$8\sigma^2 3\pi^3 9\sigma^0 4\pi^1$and $8\sigma^2 3\pi^2 9\sigma^2$	32.01
$1^1\Delta$	$8\sigma^2 3\pi^3 9\sigma^2 4\pi^1$	6.75	$1^2\Delta$	$8\sigma^2 3\pi^3 9\sigma^1 4\pi^1$	15.32	$1^3\Delta$	$8\sigma^2 3\pi^3 9\sigma^0 4\pi^1$	32.17
$1^3\Sigma^-$	$8\sigma^2 3\pi^3 9\sigma^2 4\pi^1$	6.78	$1^2\Sigma^-$	$8\sigma^2 3\pi^3 9\sigma^1 4\pi^1$	15.38	$1^1\Sigma^-$	$8\sigma^2 3\pi^3 9\sigma^0 4\pi^1$	32.28
$1^1\Sigma^-$	$8\sigma^2 3\pi^3 9\sigma^2 4\pi^1$	6.80	$3^2\Sigma^+$	$8\sigma^2 3\pi^3 9\sigma^1 4\pi^1$ and $8\sigma^2 3\pi^4 9\sigma^0 10\sigma^1$	15.77	$1^1\Delta$	$8\sigma^2 3\pi^3 9\sigma^0 4\pi^1$	32.34
$2^3\Pi$	$8\sigma^1 3\pi^4 9\sigma^2 4\pi^1$	8.31	$1^4\Pi$	$8\sigma^1 3\pi^3 9\sigma^1 4\pi^1$	16.80	$2^3\Sigma^-$	$8\sigma^2 3\pi^2 9\sigma^2$	32.82
$3^1\Sigma^+$	$8\sigma^2 3\pi^4 9\sigma^1 10\sigma^1$ and $8\sigma^2 3\pi^3 9\sigma^2 4\pi^1$	8.45	$2^4\Pi$	$8\sigma^2 3\pi^3 9\sigma^1 10\sigma^1$	17.71	$3^1\Sigma^+$	$8\sigma^2 3\pi^3 9\sigma^0 4\pi^1$	33.32
$2^1\Pi$	$8\sigma^2 3\pi^3 9\sigma^2 10\sigma^1$	8.67	$3^2\Pi$	$8\sigma^2 3\pi^3 9\sigma^1 4\pi^1$	18.02	$2^1\Delta$	$8\sigma^2 3\pi^2 9\sigma^2$	33.82
			$2^4\Sigma^+$	$8\sigma^1 3\pi^4 9\sigma^1 10\sigma^1$	19.42	$2^3\Pi$	$8\sigma^1 3\pi^3 9\sigma^2$&$8\sigma^1 3\pi^4 9\sigma^0 4\pi^1$	33.91
						$2^1\Pi$	$8\sigma^1 3\pi^4 9\sigma^0 4\pi^1$	34.73

[a] T (in eV) corresponds to MRCI + Q vertical excitation energy with respect to the AlCl $X^1\Sigma^+$ minimum (i.e., at R_{Al-Cl} = 2.140 Å, Table 2).

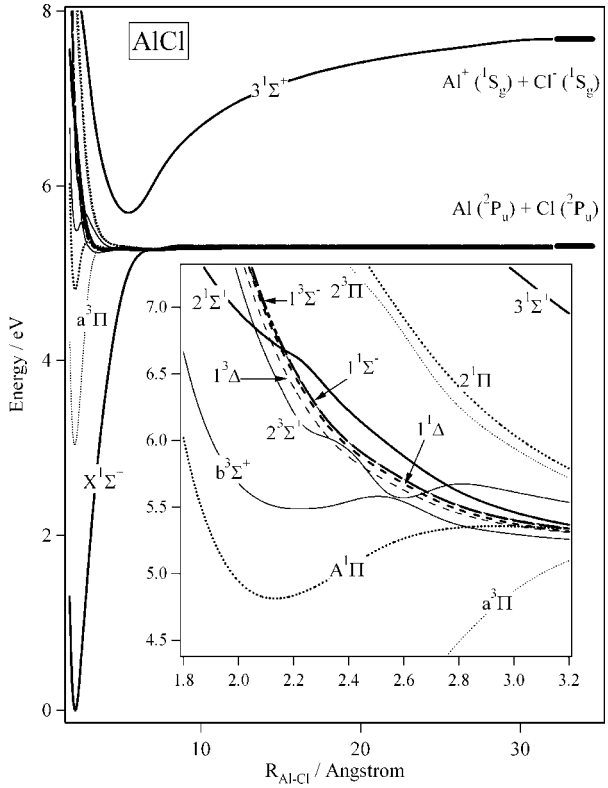

Figure 1. MRCI + Q potential-energy curves of the singlet (thick lines) and triplet (thin lines) electronic states of AlCl, correlating to the two lowest dissociation limits. The inset gives the electronic states in the 4.4−7.3 eV energy range.

eV deduced from the emission spectra of Sharma[13] and of Mahieu et al.[12] 2) The full set of curves of Figure 1 (see also the inset) shows that $^3\Delta$ is repulsive in nature, whereas a weak potential well is found for $^3\Sigma^+$ for which three vibrational levels at 129.8, 407.8, and 683.5 cm^{-1} with respect to its minimum are located.

Table 2 presents the spectroscopic constants of the electronic states of AlCl and their comparison with previous experimental and theoretical data. This includes the equilibrium distances (r_e), the rotational constants (B_e), the vibration−rotation terms (α_i), the harmonic frequencies (ω_e), and the anharmonic terms ($\omega_e x_e$, $\omega_e y_e$). This table shows that our equilibrium distances are in good agreement with previous determinations. For AlCl $X^1\Sigma^+$, our MRCI + Q computed r_e is 2.140 Å, which differs by 0.01 Å from the mw experimental value.[7] This difference reduces to 0.006 Å when compared to the theoretical data of Langhoff et al.[16] For the electronic excited states of AlCl, our calculated equilibrium distances are close to the experimental values of Sharma.[13] They are also consistent with those of Langhoff et al.,[16] but they are expected to be more accurate because they are derived from larger computations. This good accord in equilibrium distances is reflected in the rotational constants B_e. Indeed, the B_e rotational constant for the AlCl ground state is calculated to be 0.2418 cm^{-1}, which differs by ~0.0021 cm^{-1} from the mw B_e value of Wyse and Gordy.[7] Similar agreement is noticeable for the vibration−rotation α_e terms. See Table 2 for further examples. Dealing with the harmonic wavenumbers, Table 2 reveals that our computed MRCI + Q ω_e values are close to those deduced experimentally from the high-resolution infrared emission spectra of AlCl by Hedderich et al.[8] For the ground electronic state, our ω_e of 484.5 cm^{-1} differs by less than 3 cm^{-1} from the ω_e value of Hedderich and co-workers. For the upper states, the differences between the measured values and our values are in the range of 1−5 cm^{-1}. For the $3^1\Sigma^+$ state, these data are predictive in nature and are expected to be of similar accuracy. Finally, we quote in Table 2 the spin−orbit constant at equilibrium geometry (A_e) for AlCl ($a^3\Pi$). This constant was deduced from the corresponding diagonal spin−orbit integral evaluated at equilibrium and using the formula given in ref 32. This value is predictive in nature. According to our experience in computing such quantities for other molecular systems and where a direct comparison with experimental data is done, this constant should be accurate to within 6−7%.[36,37]

We turn now to the discussion of the metastability of the $A^1\Pi$ electronic state of AlCl. Eleven vibrational levels are located in the potential well of this electronic state. As pointed out in the introduction, the $A^1\Pi$ $v' \geq 10$ vibrational levels are well-known to be subject to a rapid predissociation leading to

TABLE 2: Spectroscopic Constants of AlCl, $AlCl^+$, and $AlCl^{2+}$; All Values Are in cm^{-1}, Except for r_e, which is in Angstroms

state	r_e	B_e	α_e	G_0	ω_e	$\omega_e x_e$	$\omega_e y_e$	A_e
				AlCl				
$X^1\Sigma^+$	2.140	0.2418	0.0017	239.7	484.5	6.47	−0.98	
[a]	2.146				467			
[b]					481.4	2.037	0.0036	
[c]	2.130	0.2439	0.0016		481.7	2.07		
[d]					481			
[e]	2.130	0.2477	0.0016	240.1	481.3	1.95		
[f]		0.2439	0.0016					
[g]					480.2			
[h]	2.130				481.8	2.10	0.0066	
$a^3\Pi$	2.107	0.2494	0.0015	259.7	519.1	0.52	0.23	51.6[n]
[a]	2.114				519			
[d]					520			
[f]		0.25239	0.00114					
[i]		0.25343	0.00132					
[j]	2.10	0.250	0.002		524.35	2.175		
$A^1\Pi$	2.132	0.2435	0.0027	223.9	453.0	8.03	−0.44	
[a]	2.152				449			
[b]		0.24430	0.00199		441.6	2.81	−0.309	
[d]					429			
[f]		0.24537	0.0025					
[g]					452.9	5.46	−0.14	
$b^3\Sigma^+$	2.233	0.2220	−0.0023	129.8	[k]			
[a]	2.227				246			
[f]		0.22799						
[i]		0.22858[l]						
[j]	2.21	0.226			∼350			
$3^1\Sigma^+$	5.465	0.0371	−0.00001	40.4	80.8	0.07	0.004	
				$AlCl^+$				
$X^2\Sigma^+$	2.023	0.2703	0.0014	313.1	638.6	16.65	−1.59	
[m]	2.037	0.267	0.0015		592	2.77		
$B^2\Sigma^+$	2.492	0.1782	0.0013	176.8	349.2	−2.54	0.04	
[m]	2.501	0.177	<0.0001		397	0.77		
$C^2\Pi$	2.065	0.2596	0.0026	267.0	534.9	3.23	0.19	−134.9[o]
[m]	2.066	0.259	0.0028		549	6.41		
$1^4\Sigma^+$	2.361	0.1986	0.0020	179.7	367.3	9.74	−0.28	
$1^4\Delta$	2.390	0.1938	0.0029	168.0	346.5	12.40	−0.67	76.8[p]
$1^4\Sigma^-$	2.417	0.1894	0.0040	155.2	322.6	15.59	−1.43	
$1^2\Delta$	2.411	0.1904	0.0039	157.2	327.4	16.01	−1.35	128.5[q]
$1^2\Sigma^-$	2.417	0.1894	0.0043	153.1	319.2	16.76	−1.55	
$3^2\Sigma^+$	2.530	0.1729	0.0045	90.8	167.1	−10.38	1.14	
				$AlCl^{2+}$				
$X^1\Sigma^+$	2.004	0.2757	−0.0009	287.5	584.2	11.92	−1.67	
$1^3\Pi$	2.345	0.2013	0.0019	173.3	348.3	2.92	0.03	−282.9[n]
$1^1\Pi$	2.335	0.2031	0.0014	185.1	372.4	3.29	−0.09	
$1^3\Sigma^+$	2.484	0.1794	0.0031	108.2	216.5	2.24	−0.05	
$2^1\Sigma^+$	2.135	0.2428	0.0018	252.3	505.5	2.56	0.06	
$2^3\Sigma^+$	2.221	0.2244	0.0023	214.8	432.9	5.30	−0.35	
$1^3\Delta$	2.243	0.2200	0.0018	211.4	424.6	3.14	0.23	111.1[r]
$1^1\Sigma^-$	2.289	0.2113	0.0017	189.0	380.0	3.19	0.08	
$2^3\Sigma^-$	2.353	0.2000	0.0016	266.1	537.9	8.01	0.67	
$2^1\Delta$	2.474	0.1809	0.0030	255.2	520.5	18.60	−0.86	

[a] Calcd, ref 16. [b] Expt, ref 11. [c] Expt, ref 7. [d] Expt, ref 15. [e] Calcd, ref 49. [f] Expt, ref 10. [g] Expt, ref 50. [h] Expt, ref 8. [i] Expt, ref 12. [j] Expt, ref 13. [k] This potential well supports three vibrational levels at 129.8, 407.8, and 683.5 cm^{-1} with respect to its minimum. [l] Previously mis-assigned to $b^3\Delta$ in ref 11. [m] Calcd, ref 18. [n] $A_e(^3\Pi) = <^3\Pi|H^{SO}|^3\Pi>$. [o] $A_e(^2\Pi) = 2 \times <^2\Pi|H^{SO}|^2\Pi>$. [p] $A_e(^4\Delta) = (^1/_3) \times <^4\Delta|H^{SO}|^4\Delta>$. [q] $A_e(^2\Delta) = <^2\Delta|H^{SO}|^2\Delta>$. [r] $A_e(^3\Delta) = (^1/_2) \times <^3\Delta|H^{SO}|^3\Delta>$.

Al + Cl. The most plausible mechanism for this predissociation is a spin−orbit induced predissociation of the A state by the $b^3\Sigma^+$ leading then directly to the desired products. For illustration, we display in Figure 2 the PECs of the electronic states in the vicinity of the A state and their mutual spin−orbit coupling matrix evolution along the AlCl internuclear distance. In Figure 2, we have also marked the vibrational pattern of the $A^1\Pi$ state lying in the 5.25−5.38 eV energy range. This figure shows that the $A^1\Pi$ is crossed by the $b^3\Sigma^+$ not far from the $A^1\Pi$ $v' = 10$, confirming the assumptions of Langhoff et al.[16] of the involvement of the $b^3\Sigma^+$ state in the predissociation of the A state. This however invalidates the participation of a $^1\Delta$ state in this predissociation as proposed by Mahieu et al.[11] Figure 2 shows that $<A^1\Pi|H^{SO}|b^3\Sigma^+>$ is high enough (∼130 cm^{-1} at their respective crossing, i.e., R_{AlCl} = ∼2.83 Å) to allow such predissociation.

Using the A and b potentials and our spin−orbit coupling evolution and the *BCONT* program, we calculate the spin−orbit induced predissociative lifetimes of the rovibrational levels of the $A^1\Pi$ state. The corresponding results are given in Table 3, which lists also the radiative and tunneling lifetimes of these rovibrational levels computed using the *LEVEL* program. Table

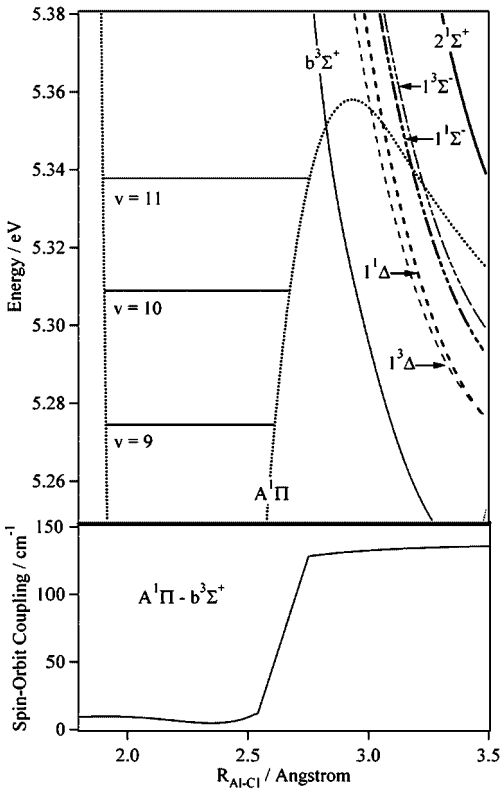

Figure 2. Top: Details of Figure 1 in the 5.25−5.38 eV energy range. We also mark the vibrational levels of the $A^1\Pi$ electronic state close to the A−b crossing (cf. text for more details). Bottom: Evolution of the $<A^1\Pi|H^{SO}|b^3\Sigma^+>$ spin−orbit coupling along the AlCl internuclear distance.

TABLE 3: Calculated Lifetimes of the AlCl ($A^1\Pi$) Rovibrational Levels

AlCl		$A^1\Pi$				
v'	N'	energy/ cm^{-1}	total lifetime	radiative	tunnelling	spin−orbit predissociation
0		223.9	5.9 ns	5.9 ns		
1		662.7	6.1 ns	6.1 ns		
2		1088.6	6.3 ns	6.3 ns		
3		1505.2	6.6 ns	6.6 ns		
4		1912.6	6.8 ns	6.8 ns		
5		2308.6	7.1 ns	7.1 ns		
6		2690.4	7.5 ns	7.5 ns		
7		3055.0	8.0 ns	8.0 ns		
8		3397.4	8.6 ns	8.6 ns		
9		3711.1	9.5 ns	9.5 ns		
10				11.0 ns		
10	0	3988.9	0.16 ns		5.36 ms	0.16 ns
10	10	4010.8	0.14 ns		2.41 ms	0.14 ns
10	20	4072.4	83.3 ps		0.29 ms	83.3 ps
10	30	4173.3	37.9 ps		13.5 μs	37.9 ps
10	32	4198.1	31.5 ps		6.8 μs	31.5 ps
10	33	4211.1	28.6 ps		4.8 μs	28.6 ps
10	34	4224.5	25.9 ps		3.4 μs	25.9 ps
10	40	4312.7	13.9 ps		0.37 μs	13.9 ps
10	50	4489.4	4.43 ps		9.0 ns	4.43 ps
11				13.5 ns		
11	0	4222.0	0.61 ps		0.71 ns	0.61 ps
11	10	4242.5	0.56 ps		0.48 ns	0.56 ps
11	20	4300.1	0.43 ps		0.17 ns	0.43 ps
11	30	4393.8	0.28 ps		37.6 ps	0.28 ps
11	40	4522.0	0.15 ps		6.3 ps	0.15 ps
11	50	4681.5	0.06 ps		1.1 ps	0.07 ps

3 shows that the $0 \leq v' \leq 9$ vibrational levels are depleted only by radiative transitions to the $X^1\Sigma^+$ ground state because they are located below the Al + Cl dissociation limit. Our computed lifetime for the $A^1\Pi$ $v' = 0$ level of 5.9 ns compares well with the experimental value of 6.4 ± 2.5 ns determined by Rogowski and Fontijn[38] and with the theoretical value of 5.17 ns of Langhoff et al.[16] The situation is quite different for the $v' = 10$ and $v' = 11$ vibrational states because predissociation, radiative processes, and tunneling through the $A^1\Pi$ potential barrier should contribute to reducing their lifetimes. For the $v' = 10$, $0 \leq N' \leq 50$ rovibrational levels, our calculations show that the tunneling and the radiative depletions contribute weakly and that the major process is the spin−orbit induced predissociation via the $b^3\Sigma^+$ state, leading to lifetimes in the 160−4 ps range. For the $A^1\Pi$ $v' = 11$, $0 \leq N' \leq 50$ rovibrational states, their lifetimes are reduced to the 0.6−0.06 ps time scale, much shorter than the radiative contribution (>13 ns), which therefore can be neglected. These lifetimes are found to be due to both tunneling and spin−orbit predissociation and not only because of predissociation as previously proposed. More interestingly, Table 3 shows that several relatively long-lived rovibrational levels are computed for the $A^1\Pi$ $v' = 10$ state especially for high N' (>33) despite that $v' = 10$, $N' = 33$ is the last rovibrational level ever observed experimentally. For instance, breaking off of branches at $N' = 33$, $v' = 10$ in the A−X emission spectrum is clearly observable in the spectra of Mahieu et al.[11] We propose the following mechanism: the AlCl $A^1\Pi$ $v' = 10$, $N' \geq 34$ rovibrational states, whenever populated, undergo rapid conversion into the close lying $A^1\Pi$ $v' = 11$ rovibrational levels, which lead to the Al + Cl products in the picosecond time scale. Accordingly, the AlCl $A^1\Pi$ ($v' = 10$, $N' \geq 34$) lifetimes given in Table 3 represent an upper limit; however, they are most likely overestimated and should be in the picosecond range rather than in the nanosecond time scale.

Finally, the lifetimes of the $a^3\Pi$ rovibrational levels should be reduced mainly by phosphorescence decay to $X^1\Sigma^+$. For the $b^3\Sigma^+$ rovibrational levels, they can fluoresce to $a^3\Pi$. Their lifetimes are estimated using the formula given in ref 32 to be ~100 ms and ~0.5 μs for the $a^3\Pi$ and the $b^3\Sigma^+$ rovibrational levels, respectively.

b. $AlCl^+$. Figure 3 displays the MRCI + Q potential-energy curves of the $AlCl^+$ electronic states lying in the 9−18 eV energy range with respect to the AlCl $X^1\Sigma^+$ minimum. In Table 1, we list the dominant electron configuration of these cationic states. These electronic states correspond mostly to the removal of an electron from a valence MO for the lowest ones and to the ejection of a valence electron and simultaneous promotion of a second one into a vacant orbital for the upper electronic states. By analyzing Figure 3, one can clearly see that several electronic states present deep potential wells for both doublet and quartet spin multiplicities. For the $X^2\Sigma^+$, $A^2\Pi$, $B^2\Sigma^+$, and $C^2\Pi$, our curves agree with those computed previously by Glenewinkel-Meyer et al.[18] However, our data represent predictions for the others (Figure 3 for more details). A high density of electronic states is also remarkable, especially at the top part of Figure 3 (inset in Figure 3 for illustration). Moreover, several crossings between these electronic states can be noticed; for instance we can cite the one between the $C^2\Pi$ and the $1^4\Sigma^+$ electronic states occurring for R_{AlCl} = ~2.45 Å. These electronic states are expected to interact mutually by spin−orbit coupling, allowing conversion from one electronic state to another and vice versa.

In Table 2, we give a full set of spectroscopic data for the bound electronic states of $AlCl^+$. Generally, we have a good accord with the equilibrium distances computed by Glenewinkel-Meyer et al.; however, a fair agreement is found concerning

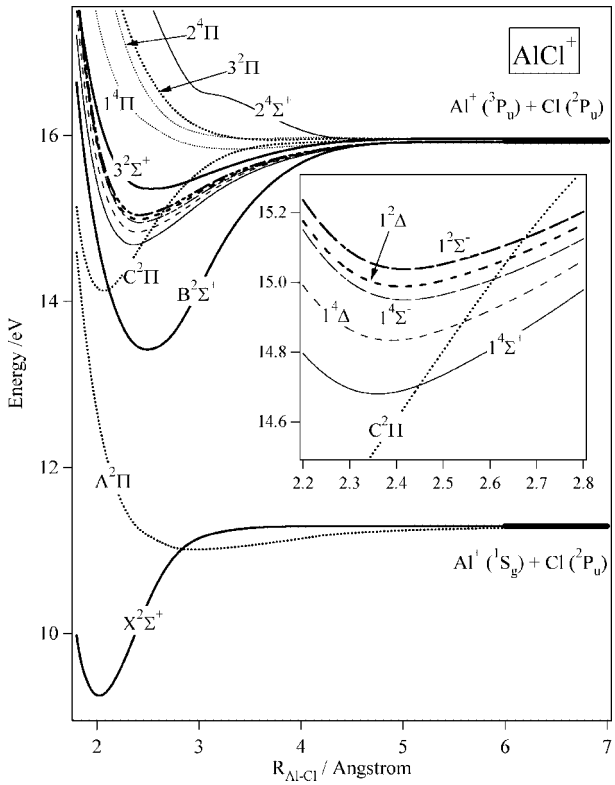

Figure 3. MRCI + Q potential-energy curves of the doublet (thick lines) and quartet (thin lines) electronic states of $AlCl^+$ correlating to the two lowest dissociation limits. Curves are presented with respect to the AlCl $X^1\Sigma^+$ minimum. The inset is giving the electronic states in the 14.5−15.3 eV energy range.

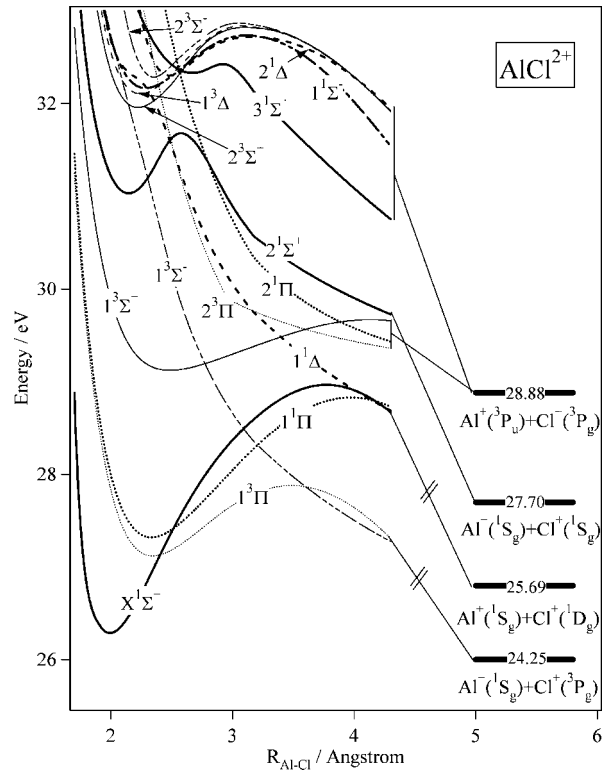

Figure 4. MRCI + Q potential-energy curves of the singlet (thick lines) and triplet (thin lines) electronic states of $AlCl^{2+}$ correlating to the four lowest dissociation limits. These potentials are given in energy with respect to the AlCl ($X^1\Sigma^+$) minimum.

the harmonic and anharmonic terms with these earlier computations. Because an excellent agreement between our cc-pwCV5Z/CASSCF/MRCI + Q and the highly accurate experimental data for the neutral molecule is observed, we believe that our predictions should be more reliable. Finally, and in contrast to the neutral molecule, the electronic states of $AlCl^+$ are most likely depleted mainly by radiative transitions. Relatively long lifetimes are computed for them. For example, the $B^2\Sigma^+$ $0 \leq v^+ \leq 10$ levels' lifetimes are computed to be in the 0.5−16.9 μs time range, whereas nanosecond−picosecond lifetimes are calculated for the A state of AlCl (above).

c. $AlCl^{2+}$. No data is found in the literature treating the $AlCl^{2+}$ dication. To fill the gap in our understanding of this molecular species, we investigated the PECs of the $AlCl^{2+}$ electronic states converging to the $Al^+(^1S_g) + Cl^+(^3P_g)$, $Al^+(^1S_g) + Cl^+(^1D_g)$, $Al^+(^1S_g) + Cl^+(^1S_g)$, and some of those converging to the $Al^+(^3P_u) + Cl^+(^3P_g)$ asymptote. The corresponding potentials are depicted in Figure 4. These PECs are presented, here again, with respect to the AlCl $X^1\Sigma^+$ minimum. Surprisingly, deep potential wells are found for several electronic states of this dication for both singlet and triplet multiplicities. These potential wells are located above their corresponding dissociation limits and are separated from them by large potential barriers, which is characteristic for molecular dications.[39] Therefore, the $AlCl^{2+}$ dication should be thermodynamically stable, as established for the isovalent molecule AlF^{2+}, which has been detected in the laboratory by Heinemann, Schroder, and Schwarz.[20] Finally, it can be obviously seen in Figure 4 that the repulsive $1^3\Sigma^-$ electronic state, which correlates to the ground dissociation limit, crosses all low-lying electronic states of $AlCl^{2+}$. Hence, this repulsive electronic state should participate in the predissociation of the bound $AlCl^{2+}$ electronic states leading at least to the $Al^+(^1S_g) + Cl^+(^3P_g)$ products.

Table 1 gives the dominant electron configuration of the electronic states displayed in this figure. When compared to the isovalent BF^{2+} dication,[40] one can clearly see that the shape of the potential-energy curves of these two dications is similar, especially for their low-lying electronic states. As for BF^{2+}, the electronic ground state of $AlCl^{2+}$ is of $^1\Sigma^+$ symmetry species. In BF^{2+}, the relative stabilization of the $^1\Sigma^+$ has been found to be due to partial donation of the B^{2+} 2s atomic orbital to the fluorine atom and to partial back-transfer of charge via the π orbitals. The situation should be similar for $AlCl^{2+}$ where a donation from the Al^{2+} 3s to the chlorine atom occurs together with a back-transfer of charge through the π system of AlCl.

For the dicationic electronic states presenting potential wells, Table 2 lists their equilibrium distances and their spectroscopic parameters. These data are predictive in nature and should be of similar accuracy as already discussed for the neutral AlCl molecule.

Let us consider now the predissociation of $AlCl^{2+}(X^1\Sigma^+, 1^3\Pi, 1^1\Pi$, and $1^3\Sigma^+)$ via the $1^3\Sigma^-$ induced by spin−orbit coupling. The corresponding spin−orbit couplings are given in Figure 5. Except for the $<1^3\Sigma^+|H^{SO}|1^3\Sigma^->$ spin−orbit matrix element, Figure 5 shows that the spin−orbit couplings between these electronic states are high enough to allow predissociation phenomena to take place. For the $AlCl^{2+}(X^1\Sigma^+)$ vibrational levels located close to its respective crossing with this repulsive state, a predissociation lifetime of ~0.4 ps is computed. For the $AlCl^{2+}(1^3\Pi)$ state, a relatively longer lifetime (~0.2 ns) is calculated here because of unfavorable overlap between the bound and the repulsive states because the $1^3\Pi-1^3\Sigma^-$ crossing takes place far from the last vibrational level of the triplet. Our calculations show that only the three upper vibrational levels of this state are weakly predissociated by the repulsive $1^3\Sigma^-$. For $AlCl^{2+}(1^1\Pi)$, the spin−orbit predissociation lifetimes reduce

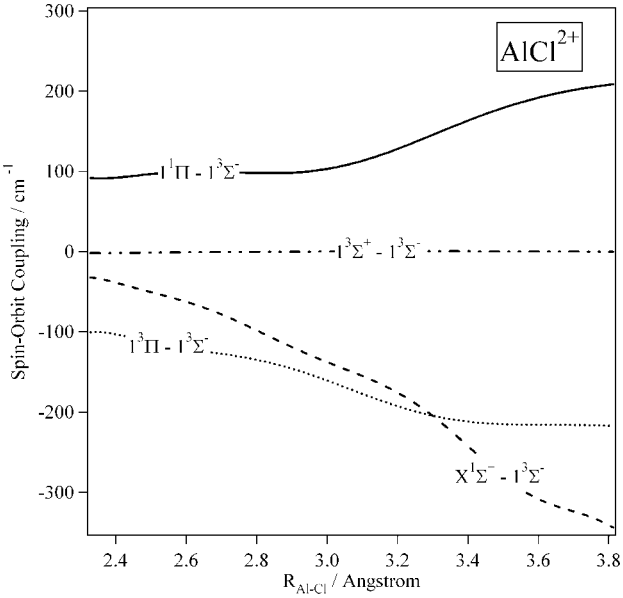

Figure 5. Spin−orbit coupling evolutions between the repulsive $1^3\Sigma^-$ and the four low-lying electronic states of $AlCl^{2+}$ along the AlCl internuclear separation. These couplings are calculated in Cartesian coordinates.

again to the 0.5 ps scale. Because of the near-zero value for $<1^3\Sigma^+|H^{SO}|1^3\Sigma^->$, the lifetimes of the $AlCl^{2+}(1^3\Sigma^+)$ rovibrational levels are increased to more than 10 ns.

d. Theoretical Single and Double Ionization Spectra of AlCl. With a view to guiding future experimental works, we have simulated the single and double ionization spectra of AlCl. These spectra were generated using the *LEVEL* program of Le Roy[33] by calculating the Franck−Condon factors of direct single and double ionization transitions between the electronic ground state $X^1\Sigma^+$ of the neutral AlCl molecule and the electronic states of $AlCl^+$ and $AlCl^{2+}$, which are accessible by photoionization. A "*Q*-branch'' approximation was adopted; that is, only transitions with $\Delta J = 0$ were considered. The validity of this approach to simulating photoionization spectra has been widely discussed previously and well demonstrated in similar works.[41−43] The single ionization spectrum of AlCl is displayed in part A of Figure 6 and the double ionization spectrum of AlCl is given in part B of Figure 6. A conventional resolution of 10 meV is used. We also considered the electronic states presenting a nonzero spin-orbit constant in our spectrum.

At the cc-pwCV5Z/CASSCF/MRCI + Q level of theory, the vertical ionization energy of AlCl is computed to be 9.37 ± 0.1 eV, which compares well with the experimental ionization energy value of 9.4 eV.[44] By photoionizing AlCl $X^1\Sigma^+$, only the doublet states of $AlCl^+$ can be reached and not the quartets. The spectrum of part A of Figure 6 consists of a well-resolved band corresponding to the $AlCl^+(X^2\Sigma^+, v^+) + e^- \leftarrow AlCl(X^1\Sigma^+, v = 0) + h\nu$ transitions. A relatively long vibrational progression is observed because of the different equilibrium distances of the initial and the final states. Then an unstructured band is located for energies of 11.4−12.3 eV corresponding to the reflection of the AlCl ground vibrational wave function into the repulsive part of the $AlCl^+$ $A^2\Pi$ potential. This part of the spectrum is in accord with the earlier simulated spectrum of Berkowitz and Dehmer.[19] For energies higher than 13.5 eV, several bands are computed because of the population of the numerous doublet $AlCl^+$ states correlating to $Al^+(^3P_u) + Cl(^2P_u)$ (above). Whenever measured, the attribution of the experimental spectra at these energies will be difficult and our predicted spectrum will be helpful.

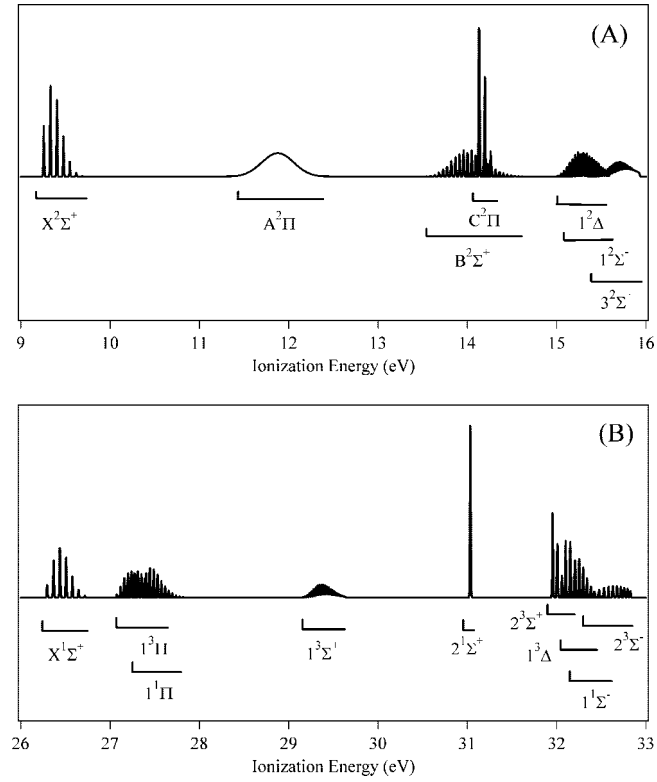

Figure 6. Simulation of the single ionization (in A) and double ionization (in B) spectra of AlCl. The Franck−Condon factors and frequencies of transitions between the $v = 0$ vibrational level of the ground electronic state of neutral AlCl and electronic states of $AlCl^+$/$AlCl^{2+}$ were calculated using the *LEVEL* program. Convolution of the output was carried out using Gaussian function with a fwhm of 10 meV to simulate the resolution achieved by current TPEsCO experiments.

For energies higher than 26.4 eV with respect to AlCl $X^1\Sigma^+$ $v = 0$, the $AlCl^{2+}$ dication can be formed after double ionizing the neutral AlCl ground state. All electronic states depicted in Figure 4 of both singlet and triplet spin-multiplicities can be accessed. The corresponding spectrum is displayed in part B of Figure 6. The first broad band corresponds to the $AlCl^{2+}$ $X^1\Sigma^+$, $v^+ + 2e^- \leftarrow$ AlCl $X^1\Sigma^+$, $v = 0 + h\nu$ transitions. As for the $AlCl^+$ ground state, a relatively long vibrational progression is observed because of the different equilibrium distances of the initial and final states. All electronic states possessing potential wells in Figure 4 contribute to this spectrum. For example, we can focus on the $2^1\Sigma^+$ electronic state at ∼31 eV, for which only one peak is computed because of similar equilibrium geometries in the initial and final states. For energies higher than 31.5 eV, several bands are computed because of the high density of electronic states. Readers are referred to part B of Figure 6 for more details.

4. Conclusion

An overall good agreement between our theoretical results and the experimental determinations for the lowest electronic states of the neutral AlCl molecule is found. This allowed reliable predictions for the so far unknown spectroscopic data for the highly excited states of AlCl and for $AlCl^+$ and $AlCl^{2+}$ to be given. Because of the importance of the AlCl molecule and related ions, we believe that our simulated single and double ionization spectra of AlCl should be of great help in understanding the spectroscopy and structure of these molecular species. These spectra correspond to the type of transitions observed in

conventional experimental methods dealing with the spectroscopy of molecular cations and dications, such as photoelectron spectroscopy (PES), threshold photoelectron techniques, threshold photoelectrons in coincidence spectroscopy (TPEsCO),[45] and time-of-flight photoelectron photoelectron coincidence (TOF-PEPECO)[46] methods. The charge-stripping spectroscopy applied to the $AlCl^+$ species[20] should also provide reliable data on the $AlCl^{2+}$ dication that can be compared directly to our theoretical results. In the laboratory, the neutral AlCl diatomic molecule can be easily produced in the gas phase from $AlCl_3$ either by heating neat $AlCl_3$ or a mixture of $AlCl_3$ and aluminum.[3,4] It can also be obtained by electrical discharge or by microwave discharge in $AlCl_3$.[11,12] Aluminum monochloride vapor may also be formed by direct hydrogen reduction of the $AlCl_3 + H_2$ gas mixture at 1000 °C[47] or after reaction between aluminum and Cl_2.[48]

Acknowledgment. Professor R. J. Le Roy is acknowledged for kindly providing us with the LEVEL and BCONT programs. D.H. thanks the Ministère de l'Enseignement Supérieur et de la Recherche Scientifique of Algeria for a fellowship for a research stay at the Université Paris-Est. Dr. C. Houchins (UC Davis) is thanked for critical reading of the manuscript.

References and Notes

(1) Cernicharo, J.; Guélin, M. *Astron. Astrophys.* **1987**, *183*, L10.
(2) McGregor, W. K.; Drakes, J. A.; Beale, K. S.; Sherrell, F. G. Proceedings of the 27th Thermophysics Conference, Nashville, TN, July 1992; paper AIAA-92−2917, AIAA.
(3) Bhaduri, B. N.; Fowler, A. *Proc. R. Soc. Ser. A* **1934**, *145*, 321.
(4) Mahanti, P. C. *Z. Phys.* **1934**, *88*, 550.
(5) Lide, D. R., Jr. *J. Chem. Phys.* **1965**, *42*, 1013.
(6) Wyse, F. C.; Gordy, W.; Pearson, E. F. *J. Chem. Phys.* **1970**, *52*, 3887.
(7) Wyse, F. C.; Gordy, W. *J. Chem. Phys.* **1972**, *56*, 2130.
(8) Hedderich, H. G.; Dulick, M.; Bernath, P. F. *J. Chem. Phys.* **1993**, *99*, 8363.
(9) Hildenbrand, D. L.; Theard, L. P. *J. Chem. Phys.* **1969**, *50*, 5350.
(10) Ram, R. S.; Rai, S. B.; Upadhya, K. N.; Rai, D. K. *Phys. Scr.* **1982**, *26*, 383.
(11) Mahieu, E.; Dubois, I.; Bredohl, H. *J. Mol. Spectrosc.* **1989**, *134*, 317.
(12) Mahieu, E.; Dubois, I.; Bredohl, H. *J. Mol. Spectrosc.* **1989**, *138*, 264.
(13) Sharma, D. *Astrophys. J.* **1951**, *113*, 210.
(14) Saksena, M. D.; Dixit, V. S.; Singh, M. *J. Mol. Spectrosc.* **1998**, *187*, 1.
(15) Dearden, D. V.; Johnson, R. D., III; Hudgens, J. W. *J. Chem. Phys.* **1993**, *99*, 7521.
(16) Langhoff, S. R.; Bauschlicher, C. W., Jr.; Taylor, P. R. *J. Chem. Phys.* **1988**, *88*, 5715.
(17) Glenewinkel-Meyer, Th.; Kowalski, A.; Müller, B.; Ottinger, Ch.; Breckenridge, W. H. *J. Chem. Phys.* **1989**, *89*, 7112.
(18) Glenewinkel-Meyer, Th.; Müller, B.; Ottinger, Ch.; Rosmus, P.; Knowles, P. J.; Werner, H.-J. *J. Chem. Phys.* **1991**, *95*, 5133.
(19) Berkowitz, J.; Dehmer, J. L. *J. Chem. Phys.* **1972**, *57*, 3194, and references therein.
(20) Heinemann, C.; Schroder, D.; Schwarz, H. *J. Phys. Chem.* **1995**, *99*, 16195.
(21) Peterson, K. A.; Dunning, T. H., Jr. *J. Chem. Phys.* **2002**, *117*, 10548.
(22) Basis sets were obtained from the Extensible Computational Chemistry Environment Basis Set Database, Version 02/02/06, as developed and distributed by the Molecular Science Computing Facility, Environmental and Molecular Sciences Laboratory, which is part of the Pacific Northwest Laboratory, P.O. Box 999, Richland, Washington 99352, USA, and funded by the U.S. Department of Energy. The Pacific Northwest Laboratory is a multi-program laboratory operated by Battelle Memorial Institute for the U.S. Department of Energy under contract DE-AC06−76RLO 1830. Contact Karen Schuchardt for further information.
(23) Knowles, P. J.; Werner, H.-J. *Chem. Phys. Lett.* **1985**, *115*, 259.
(24) Werner, H.-J.; Knowles, P. J. *J. Chem. Phys.* **1988**, *89*, 5803.
(25) Knowles, P. J.; Werner, H.-J. *Chem. Phys. Lett.* **1988**, *145*, 514.
(26) *MOLPRO* is a package of ab initio programs written by H.-J. Werner and P. J. Knowles. See http://www.molpro.net for more details.
(27) Cooley, J. W. *Math. Comput.* **1961**, *15*, 363.
(28) Langhoff, S. R.; Davidson, E. R. *Int. J. Quantum Chem.* **1974**, *8*, 61.
(29) Bauschlicher, C. W., Jr.; Partridge, H. *Chem. Phys. Lett.* **2001**, *342*, 441.
(30) Bauschlicher, C. W., Jr.; Gutsev, G. L. *J. Chem. Phys.* **2002**, *116*, 3659.
(31) Dunning, T. H., Jr.; Peterson, K. A.; Wilson, A. K. *J. Chem. Phys.* **2001**, *114*, 9244.
(32) Lefebvre-Brion, H.; Field, R. W. *The Spectra and Dynamics of Diatomic Molecules*; Elsevier: New York, 2004.
(33) Le Roy, R. J. *LEVEL 8.0: A Computer Program for Solving the Radial Schrödinger Equation for Bound and Quasibound Levels*; University of Waterloo Chemical Physics Research Report CP-663, 2007; http://leroy.uwaterloo.ca.
(34) Le Roy, R. J.; Kraemer, G. T. *BCONT 2.2. Computer Program for Calculating Absorption Coefficients, Emission Intensities or (Gold Rule) Predissociation Rates*; University of Waterloo Chemical Physics Research Report CP-650R^2, 2004. The source code and manual for this program may be obtained from "Computer Programs" link at http://leroy.uwaterloo.ca.
(35) Emsley, J. *The Elements*, Second Edition; Clarendon Press: Oxford, 1991.
(36) Hochlaf, M.; Eland, J. H. D. *J. Chem. Phys.* **2004**, *120*, 6449.
(37) Hochlaf, M.; Chambaud, G.; Rosmus, P.; Andersen, T.; Werner, H.-J. *J. Chem. Phys.* **1999**, *110*, 11835.
(38) Rogowski, D. F.; Fontijn, A. *Chem. Phys. Lett.* **1987**, *137*, 219.
(39) Hochlaf, M.; Palaudoux, J.; Ben Houria, A. Transworld Research Network. *Rec. Res. Dev. Chem. Phys.* **2004**, *5*, 403.
(40) Kolbuszewski, M.; Wright, J. S.; Buenker, R. J. *J. Chem. Phys.* **1995**, *102*, 7519.
(41) Bennett, F. R.; Critchley, A. D. J.; King, G. C.; Le Roy, R. J.; McNab, I. R. *Mol. Phys.* **1999**, *97*, 35.
(42) Yencha, A. J.; Juarez, A. M.; Lee, S. P.; King, G. C.; Bennett, F. R.; Kemp, F.; McNab, I. R. *Chem. Phys.* **2004**, *303*, 179.
(43) Ben Houria, A.; Ben Lakhdar, Z.; Hochlaf, M.; Kemp, F.; McNab, I. R. *J. Chem. Phys.* **2005**, *122*, 054303.
(44) Hildenbrand, D. L. *J. Chem. Phys.* **1977**, *66*, 3526.
(45) Hochlaf, M.; Kjeldsen, H.; Penent, F.; Hall, R. I.; Lablanquie, P.; Lavollée, M.; Eland, J. H. D. *Can. J. Phys.* **1996**, *74*, 856.
(46) Eland, J. H. D. *Chem. Phys.* **2003**, *294*, 171.
(47) Araki, T.; Motojima, S. *Mater. Sci. Eng., B* **1996**, *39*, L1.
(48) Rosenwaks, S. *J. Chem. Phys.* **1976**, *65*, 3668.
(49) Behere, S. H.; Sardesai, P. L. *Indian J. Pure Appl. Phys.* **1982**, *20*, 693.
(50) Kumar, Y.; Khanna, B. N.; Varshney, D. C. *Indian J. Pure Appl. Phys.* **1985**, *23*, 128.

JP805508F